Statistical Ga clusters and A_1(TO) gap mode in $Al_xGa_{1-x}N$ alloys

A. A. Klochikhin,[1,2] V. Yu. Davydov,[1] I. N. Goncharuk,[1] A. N. Smirnov,[1] A. E. Nikolaev,[1] and M. V. Baidakova[1]
[1]*Ioffe Physico-Technical Institute, St. Petersburg 194021, Russia*
[2] *Petersburg Nuclear Physics Institute, Gatchina, St. Petersburg 188350, Russia*

J. Aderhold, J. Graul, J. Stemmer, and O. Semchinova
LFI Universität Hannover, Schneiderberg 32, 30167 Hannover, Germany
(Received 8 February 2000)

Results of a comprehensive study of the behavior of the A_1(TO) phonon mode in hexagonal $Al_xGa_{1-x}N$ alloys in the entire compositional range are described. It has been found that the Raman spectrum of $Al_xGa_{1-x}N$, with a Ga content $(1-x)<0.3$, exhibits a large broadening with a complex structure. We attribute this structure to a manifestation of the phonon density of states in the region of vibrations of the optical A_1(TO) branch, and to the appearance of a gap mode in AlN. Both effects are due to the substitution of heavier Ga atoms in the cation sublattice of AlN. A theoretical approach is suggested which describes changes in the vibrational spectrum at a sufficiently strong perturbation resulting from isoelectron substitution. In the framework of the developed model, the dependence of the intensity and band shape of the gap mode on Ga content are calculated and compared with the experimental Raman data. The experimental and theoretical dependences are shown to be in good agreement in the region $(1-x)<0.12$–0.15. The obtained results indicate that the formation of an A_1(TO) gap mode in the regions of low and intermediate Ga contents is caused by statistical Ga clusters in the cation sublattice of the solid solution. In a limited range of Ga contents, the behavior of the A_1(TO) phonon mode in $Al_xGa_{1-x}N$ can be considered as a two-mode behavior.

I. INTRODUCTION

Wide-gap semiconductors GaN and AlN, and their solid solutions ($Al_xGa_{1-x}N$), are known to be promising materials for optical applications, especially for light emission in the blue and ultraviolet ranges.[1,2] Progress in the growth of nitrides has stimulated basic research into these materials. However, compared to the considerable amount of research done on GaN, the alloy system $Al_xGa_{1-x}N$ has received much less attention. To obtain a deeper insight into the transport and thermal properties of this material, as well as its phonon-assisted optical transitions, its crystalline lattice dynamics should be thoroughly studied.

Special attention was paid to the vibrational spectrum of disordered systems.[3–11] Among the methods used to describe the lattice dynamics of alloys is the self-consistent coherent potential approach,[9] the phenomenological random-element-isodisplacement (REI) method, and the modified random-element-isodisplacement (MREI)[10,11] method. According to the REI and MREI models, ternary alloys are divided into two main classes (one- and two-mode models) depending on the behavior of optical phonons at the Γ point. In Refs. 10 and 11, criteria for the behavior of optical phonons at the Γ point, allowing a correct prediction of the type of the solid solution, were suggested. If the ratio of the difference between the optical band energies of two individual components to the width of the energy band is large, a ternary alloy exhibits a two-mode behavior. Conversely, if the bands of pure components overlap in the energy space, the ternary alloy is a one-mode model. In the case of an ideal one-mode-type behavior, frequencies of different optical modes vary continuously and approximately linearly with varying alloy composition. On the other hand, in typical two-mode type behavior two sets of optical modes are observed, each set corresponding to one of two components of the alloy.

The local and gap modes can be observed in the spectra of two-mode-type crystals when the content of one of the components is much greater than that of the other. For the gap mode to occur, there must be a frequency gap between the acoustic and optic bands. It was noted in Refs. 10 and 11 that in some cases a local mode can rise out of the top, and a gap mode can fall out of the bottom of the optical branch when the top or bottom of the band takes place at an arbitrary point of the Brillouin zone.

Solid solutions of $Al_xGa_{1-x}N$, as well as pure crystals of GaN and AlN, crystallize in two polytypes: cubic and hexagonal. The behavior of phonons in cubic $Al_xGa_{1-x}N$ was theoretically considered in Refs. 12 and 13. It was found that LO phonon must exhibit a one-mode type behavior, while the behavior of the TO phonon must show two-mode behavior. These predictions were confirmed by Raman-scattering data for cubic $Al_xGa_{1-x}N$ alloys.[14] For hexagonal $Al_xGa_{1-x}N$, theoretical studies of the phonon mode behavior have been carried out only for A_1 and E_1 phonons, which are polar phonons.[13,15,16] In these works, the one-mode behavior of the A_1(LO) and E_1(LO) phonons was predicted. However, there was a discrepancy in the results concerning the TO-phonon behavior. In Ref. 15 the one-mode behavior of the A_1(TO) and E_1(TO) phonons was derived from the MREI model for hexagonal $Al_xGa_{1-x}N$, while in Ref. 13 the two-mode behavior of these phonons (similar to transverse phonons in the cubic polytype) was predicted.

The experimental data on hexagonal $Al_xGa_{1-x}N$ are also rather contradictory. In earlier works,[17,18] a one-mode-type behavior was found from Raman measurements for all optical phonons in the case of a small Al content $(0<x<0.15)$.

In more recent works,[16,19] the phonon behavior was traced for the whole compositional range ($0<x<1$). The Raman data obtained in these works speak in favor of an apparent one-mode behavior of the longitudinal and transverse components of A_1 and E_1 polar modes. They also suggest a two-mode behavior of the E_2(high) nonpolar mode. Zone-center modes in hexagonal $Al_xGa_{1-x}N$ were also studied by infrared spectroscopy. Recent IR reflectivity measurements for $Al_xGa_{1-x}N$ in the whole compositional range ($0<x<1$) indicated the one-mode behavior of the E_1(LO) phonons and the two-mode behavior of the E_1(TO) phonons.[20] Neither Al local mode in GaN nor Ga gap mode in AlN have been found by both techniques.

Thus the experimental data are consistent with the theoretical predictions of the one-mode behavior of the LO phonon modes in hexagonal $Al_xGa_{1-x}N$. However, as concerns the behavior of the transverse optical modes, there is a significant disagreement between the results of different works both in theory and experiment.

In this paper we describe the results of detailed experimental and theoretical studies of the behavior of the phonon mode of the A_1(TO) symmetry in hexagonal $Al_xGa_{1-x}N$. In spite of an increasing number of investigations of the lattice dynamics of solid solutions based on the theories of Refs. 10 and 11, the microscopical mechanism underlying the two-mode behavior still remains rather puzzling. Here we present an attempt at a microscopical approach to the problem of two-mode behavior in the limit of low and intermediate Ga contents in the hexagonal $Al_xGa_{1-x}N$ solid solution, assuming (i) a random distribution of substituting atoms, (ii) an arbitrary position of the top or bottom of an optical band in the Brillouin zone, (iii) a strong enough perturbation to split off a local or a gap mode, and (iv) a relatively small concentration of the active component (Ga in our case), which is less than the percolation concentration over the perturbed sublattice sites. The last restriction means that only clusters of a finite size can exist in a perturbed sublattice.[21–23]

To simplify numerical calculations, we use two assumptions: (1) only changes in the mass of a substituting atom are taken into account, while the force constants remain the same; and (2) the number of clusters at a given concentration can be found for the $Al_xGa_{1-x}N$ alloy using the results available for the fcc lattice and neglecting, therefore, a small difference between the wurtzite and zinc-blende lattices.

We attribute the observed changes in the Raman spectrum of the A_1(TO) phonon mode of $Al_xGa_{1-x}N$ in the region $(1-x)<0.2$ to the formation of statistical Ga clusters in the case of a random distribution of these atoms over the cation sublattice sites. The averaged number of clusters for the fcc sublattice for an arbitrary concentration obtained in Ref. 24 is used to estimate the density of gap states and its dependence on concentration.

The structure of the paper is as follows. The samples and experimental procedure are described in Sec. II. In Sec. III, Raman spectroscopic data on the behavior of A_1(TO) phonon mode in $Al_xGa_{1-x}N$ solid solutions in the entire compositional range ($0<x<1$) are presented. Special attention is paid to experimental investigations of the behavior of this phonon mode in Al-rich alloys. It is shown that for a Ga content $(1-x)<0.2$ a gap mode splits off the bottom of the A_1(TO) branch, which probably occurs at the H point of the Brillouin zone. Section IV is devoted to the theoretical consideration of the disordered lattice vibration problem when the perturbation at substitution is strong enough to produce a local mode or a gap mode. This approach assumes that the active component concentration is lower than the critical concentration for percolation over the fcc sublattice sites. The model calculations of density of the gap states split off the bottom of the A_1(TO) branch are performed and compared with experiment. Section V contains summary remarks.

II. EXPERIMENT AND SAMPLES

A large set of $Al_xGa_{1-x}N$ samples with a difference in the Al content of not more than 3–5% in the entire compositional range ($0<x<1$), as well as AlN and GaN layers, were used for the study. 0.5-μm-thick $Al_xGa_{1-x}N$ layers in the compositional range $0<x<0.5$ were grown on thin GaN buffer layers deposited on the *c*-plane sapphire in a Riber 32 molecular-beam epitaxy system. The 1–2-μm-thick layers of $Al_xGa_{1-x}N$ alloys in the composition range $0.5<x<1$ were grown by hydride vapor phase epitaxy on a (111) silicon substrate without a buffer layer. The details of the growth can be found in Refs. 25 and 26. The structural quality of the layers and the alloy composition were controlled by x-ray diffraction and electron probe microanalysis. Raman spectra of the samples were measured in a backscattering configuration at room temperature and at 100 K. An Ar^+ laser ($\lambda = 488$ nm) was used as a source of excitation.

III. EXPERIMENTAL RESULTS

A. Phonons in perfect GaN and AlN

Hexagonal GaN, AlN, and $Al_xGa_{1-x}N$ alloys crystallize in the wurtzite structure belonging to the C_{6v}^4 ($P6_3mc$) space group. According to the factor group analysis at the Γ point, phonon modes in a hexagonal crystal belong to the irreducible representations. $\Gamma_{ac}+\Gamma_{opt}=(A_1+E_1)+(A_1+2B_1+E_1+2E_2)$. Among optical phonons, the A_1 and E_1 modes are both Raman and IR active, the E_2 modes are only Raman active, and the B_1 modes are silent.[27] There are six optical modes $[1A_1(\mathrm{TO})+1A_1(\mathrm{LO})+1E_1(\mathrm{TO})+1E_1(\mathrm{LO})+2E_2]$ active in the first-order Raman scattering. The Γ-point phonon frequencies are well studied both for GaN and AlN.[28–31]

Figures 1 and 2 show the behavior of phonon branches throughout the Brillouin zone and the one-phonon density of states functions (DOS) for GaN and AlN crystals, which we calculated earlier by using a phenomenological model based on short-range interatomic potentials and rigid-ion Coulomb interactions.[31] The calculated DOS function is in a good agreement with recent results of neutron experiments for GaN and AlN, and the dispersion relations are consistent with *ab initio* lattice-dynamics calculations.[32,33] It is evident from Figs. 1 and 2 that GaN has a large phonon gap (between 330 and 530 cm^{-1}), whereas AlN has a rather narrow gap (between 550 and 600 cm^{-1}). Note that the calculated dispersion curves for optical phonons of AlN have minima for some points in the Brillouin zone. Their energies are lower than the energy of the optical phonon of the A_1(TO) symmetry at the Γ point.

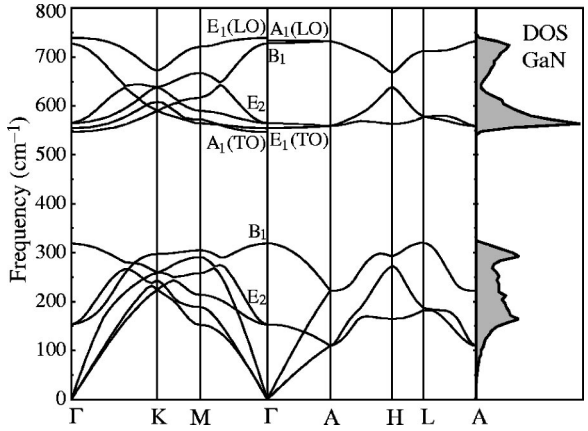

FIG. 1. Calculated phonon-dispersion curves and phonon DOS for bulk GaN.

B. A_1(TO) phonon mode behavior in $Al_xGa_{1-x}N$ alloys

Earlier only $Al_xGa_{1-x}N$ layers grown on sapphire were studied. However, the Raman spectra of sapphire and some compositions of $Al_xGa_{1-x}N$ alloys have lines at close frequencies, which creates difficulties in identifying the phonon positions in $Al_xGa_{1-x}N$. In our study the $Al_xGa_{1-x}N$ alloys were grown not only on sapphire, but also on Si substrates. In contrast to sapphire, silicon does not exhibit any strong Raman lines coinciding with the $Al_xGa_{1-x}N$ phonon modes. This provides the basis for a more reliable identification of frequency positions of phonon modes in $Al_xGa_{1-x}N$.

According to the x-ray data, all samples were single-crystal layers of the hexagonal modification without any polycrystalline inclusions or phase separation. Figure 3 shows x-ray diffractograms obtained for different alloy compositions. The double-peak structure shown in the diffractograms for the (0004) reflex is due to the $K\alpha_1$ and $K\alpha_2$ lines of Cu. The well-defined double-peak structure for all samples in the compositional range $0<x<1$ points to a good structural perfection. It should be emphasized that the diffraction curves are symmetrical for all samples, which is evidence of the absence of macrogradients (such as nonuniform distribution of defects and impurities in the samples).

On the whole, the measured first-order polarized Raman spectra were found to be consistent with selection rules for the wurtzite structure in the entire compositional range $0<x<1$. At the same time, we found that the general pattern of the mode behavior for the Al-rich compositional range is much more complicated.

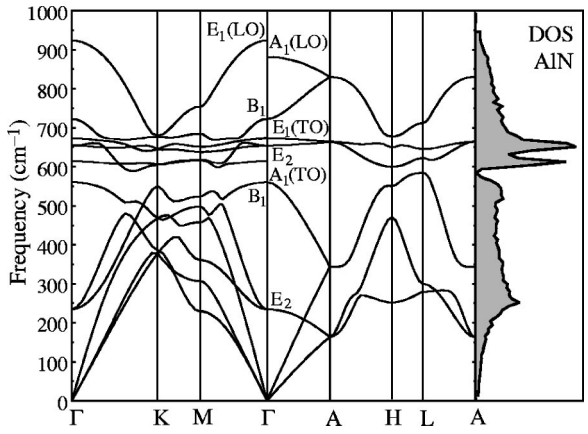

FIG. 2. Calculated phonon-dispersion curves and phonon DOS for bulk AlN.

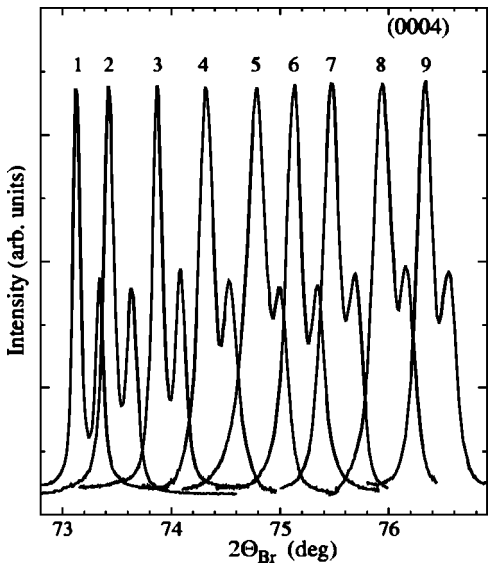

FIG. 3. High-resolution x-ray-diffraction spectra for $Al_xGa_{1-x}N$ alloys with different Al contents [x=0.08 (1), 0.14 (2), 0.28 (3), 0.40 (4), 0.54 (5), 0.65 (6), 0.74 (7), 0.87 (8), and 0.97 (9)].

Here we consider in detail the behavior of A_1(TO) phonon mode in $Al_xGa_{1-x}N$ solid solutions. We have found that this mode manifests itself in the Ga-rich compositional range as a single line which experiences a high-frequency shift with increasing Al content, and whose width remains nearly the same in a wide compositional range $0\leqslant x<0.4$, consistent with other works.[16,19] At high Al contents, this line exhibits an asymmetric broadening toward higher frequencies, the low-frequency edge remaining as sharp as before. In addition, at the high-frequency edge of this band two features appear. They change their positions and shapes as the composition of the solid solution is varied. Careful analysis has shown that these features are inherent in the polarized spectrum corresponding to the A_1(TO) phonon; they are not due to the interference from other polarizations. To illustrate this, Fig. 4 shows polarized Raman spectra in a frequency range corresponding to phonons of A_1(TO), E_1(TO), and E_2(high) symmetries for pure AlN, and two compositions of $Al_xGa_{1-x}N$ with $x=0.92$ and $x=0.78$.

Figure 5 depicts the transformation of the Raman spectrum in the compositional range $0.6<x\leqslant 1$. It is clearly seen that the intensity of the most high-frequency feature in the spectrum (circles) grows with increasing Al content, while the low-frequency peak (triangles) becomes less intense. In the limit of very high Al concentrations the low-frequency peak is a weak feature, with a maximum at 595 cm^{-1}. With increasing Al content the high-frequency feature becomes narrower, shifts toward lower frequencies, and in the limit tends toward the position typical of the A_1(TO) phonon in AlN. For pure AlN, only a single line corresponding to the A_1(TO) phonon at 611 cm^{-1} is detected in the spectrum. Concerning the third feature (diamonds) occupying the position between the features discussed above, it seems that its

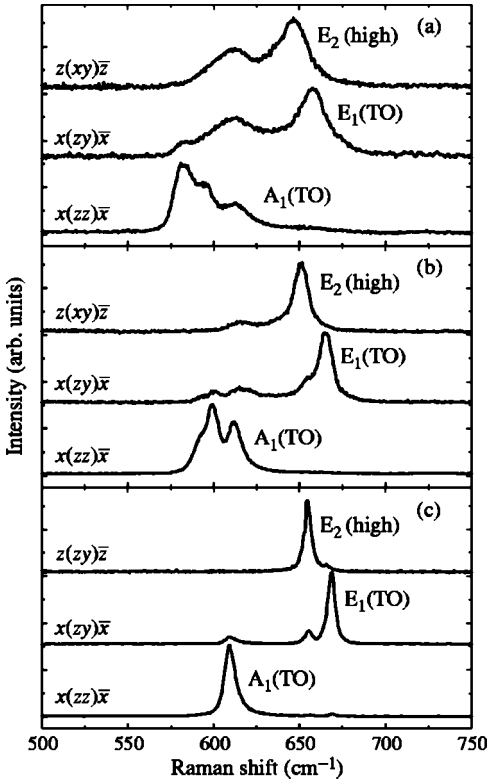

FIG. 4. Room-temperature-polarized Raman spectra for two compositions of $Al_xGa_{1-x}N$: $x=0.78$ (a), $x=0.92$ (b), and pure AlN (c) in the frequency range corresponding to phonons of A_1(TO), E_1(TO), and E_2(high) symmetry. In Porto's notation the z direction is along the c axis of the wurtzite structure, and x and y are mutually orthogonal and lie in the plane normal to the z direction.

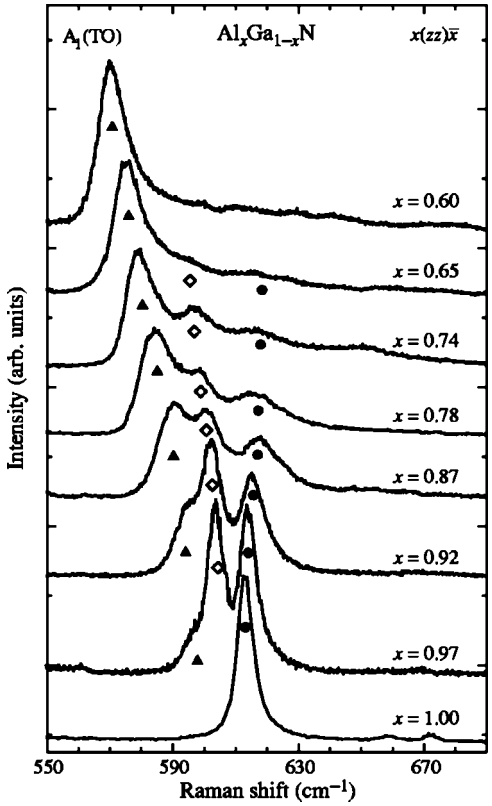

FIG. 5. Raman spectra at 100 K in the scattering configuration corresponding to the A_1(TO) phonon for $Al_xGa_{1-x}N$ with different Al contents $0.6 \leqslant x \leqslant 1$. The spectra are normalized in such a manner (except the spectrum for pure AlN) that their integral intensities are equal.

relative intensity has a weak dependence on Al content within the compositional interval $0.87<x<1$, where all three lines are well resolved.

Figure 6 shows positions of the maxima detected in the scattering configuration corresponding to the phonon mode of the A_1(TO) symmetry as a function of Al content. The spectrum transformation described above can be understood if we assume that the two lines with the opposite dependences of intensities on the Al content are GaN-like and AlN-like phonon modes of A_1(TO) symmetry. This conclusion is consistent with the theoretical predictions of the two-mode behavior of the A_1(TO) phonon given in Ref. 13.

As evidenced by our polarization measurements, the band observed between the GaN- and AlN-like phonon modes cannot be interpreted as resulting from modes belonging to other symmetries. The phase-separation tendency should be ruled out as well, according to the x-ray data. In our opinion, this band can be attributed to the manifestation of the phonon DOS associated with an extrema whose energy is lower than that of the Γ-point A_1(TO) phonon.

Phonons with arbitrary wave vectors can be active in first-order Raman scattering if electron states are affected by composition fluctuations in the solid solution or by impurities introduced into the crystal.[34–36] In this case an additional mechanism of the first-order Raman process appears. It is characterized by a violation of wave vector conservation law due to scattering or localization of intermediate exciton states by fluctuation potential. As a result, the Raman spectrum reproduces the density of states of a phonon branch rather than its spectral DOS (i.e., phonons from the Γ point).

The calculated spectrum of phonon branches throughout the Brillouin zone for AlN (Fig. 2) shows that an appropriate minimum of the dispersion curve is situated at the H point. In this case the spectral peak observed between two modes of the A_1(TO) symmetry can be regarded as a manifestation of the DOS in the region of the lower edge of this branch due to the influence of heavy Ga atoms. This effect is bound to take place if the perturbation of the vibrational spectrum due to substitution is strong enough, and can be accompanied by a splitting off of the gap mode.[37]

It is interesting to note that the Raman spectrum in the region of the A_1(TO) phonon in $Al_xGa_{1-x}N$ is much more composition sensitive for low and intermediate Ga concentrations than for low and intermediate Al concentrations. This fact shows that the perturbation of phonon states near the lower border of the A_1(TO) branch, produced by substitution of a heavier Ga atom, is stronger than the perturbation by the lighter Al atom near the same border at low Al concentrations. There are two general factors which regulate the scale of perturbation at substitution. These are the magnitude and sign of the perturbation amplitude. The sign of the perturbation amplitude below the bottom of the optical branch due to the substitution of a heavier atom can be characterized as ''attractive.'' It always leads to an enhancement of the DOS near the border, and can cause a splitting off of the gap phonon state from the band bottom if the perturbation is

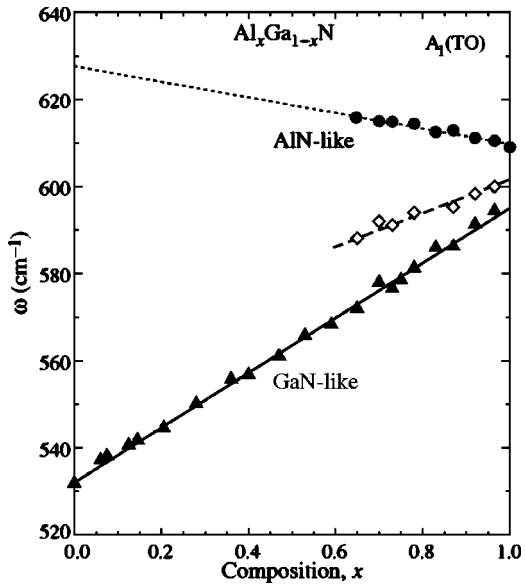

FIG. 6. Frequencies of phonon modes in the scattering configuration corresponding to the A_1(TO) phonon for $Al_xGa_{1-x}N$ as a function of Al content. Triangles show the positions of the GaN-like A_1(TO) mode, circles indicate the positions of the AlN-like A_1(TO) mode, and diamonds show the positions of the enhanced phonon DOS. The solid line corresponds to a fitting with equation $\omega_{A_1(\mathrm{TO})}=532.5+58x+55x^2$.

stronger than the critical value, i.e., the value of the single site perturbation which leads to the splitting off of the gap or localized state with the zeroth localization energy.

At a large Ga concentration the Al atoms play the major role in the scattering of phonons. The lighter atom near the same band border produces a perturbation which has a ''repulsive'' character, and gives rise only to a scattering of phonons and to a decrease in the DOS in this region. As a rule, the perturbation of the phonon motion by a given substitution has opposite signs at opposite borders of a given optical branch.

Single-site fluctuations in solid solutions produce a phonon-scattering cross section which is proportional to the product $x(1-x)$. However, this cross section is symmetrical in x and $(1-x)$ only in the first Born approximation, which is not appropriate for a large attractive perturbation. Even the coherent potential approximation shows a detectable asymmetry of the composition dependence of the phonon-scattering characteristics.[37] This becomes even more pronounced if there is a scattering of phonons on clusters of substituted atoms with an attractive sign of interaction. The number and the spatial size of fluctuations have the optimal magnitudes in the region of ''percolation concentration'' of the atoms with the attractive sign of the scattering amplitude.

In case of the A_1(TO) branch in $Al_xGa_{1-x}N$ solid solutions, the maximal effects of both the phonon scattering and localization occur in the region of $(1-x)\approx 0.15$–0.25. This range corresponds well to the value of percolation concentration for the fcc lattice, $(1-x)=0.2$, which has the same coordination number as the real cation sublattice of the solid solution.

Estimates of the intensity of the low-frequency GaN-like peak (Fig. 5) have shown that it increases approximately proportionally to the Ga content below $(1-x)=0.2$. This fact suggests that this feature of the spectrum can be regarded as the DOS of the gap mode split off from the bottom of the A_1(TO) phonon branch due to the substitution of Ga for Al. In the next sections the gap mode problem is considered theoretically, and results of numerical calculations are described.

IV. THEORETICAL CONSIDERATION

For convenience, in this section we introduce a notation for the variable concentration of the solid solution components, namely, we denote the concentration of Ga—an active component of the disordered system—by c instead of $(1-x)$, and that of Al by $(1-c)$ instead of x. We restrict our consideration to $c\leqslant 0.2$, supposing that the disorder of the perturbed sublattice can be described in terms of the fcc sublattice. The value $c=0.2$ coincides with high accuracy with the critical concentration over the fcc sublattice sites, and below this value the substitution atoms can form only clusters of finite size. We also admit that the distribution of the substitution atoms over sublattice sites is close to the random one.

Below we consider the general aspects of a calculation of a disordered system spectrum in the region of localized or gap states within the framework of the simple lattice Hamiltonian. The numerical calculations of the band shape of the gap states and a composition dependence of their integral density will be performed using a continuum Hamiltonian based on the Taylor series expansion of the phonon frequency in the wave-vector space near the Van Hove singularity. The obtained results will be used to illustrate experimental data.

A. Model Hamiltonian and the density of states of a disordered crystal

Let us consider a crystal consisting of N elementary cells with r atoms in each of them. We assume that cN lattice sites of one of sublattices are randomly filled with two sorts of atoms A and B. The average number of atoms A and B is $N_A=cN$ and $N_B=(1-c)N$, respectively. Following Refs. 4–6, the Hamiltonian that describes the vibration motion of the system in the harmonic approximation can be given by

$$H=\sum_{lk\alpha}\frac{p_\alpha^2(l,k)}{2M_{lk}}+\frac{1}{2}\sum_{lk\alpha}\sum_{l'k'\beta}\phi_{\alpha\beta}(lk;l'k')u_\alpha(lk)u_\beta(l'k'). \tag{1}$$

Here $u_\alpha(lk)=u_\alpha(lk,t)$ is the projection of the time-dependent displacement of atom k in the elementary cell l on the α axis; $p_\alpha(l,k)=M_{lk}\dot{u}_\alpha(lk)$ is the corresponding projection of the momentum of the atom; M_{lk} is its mass; and $\phi_{\alpha\beta}(lk;l'k')$ is the matrix of atomic force constants. The equation of motion which defines the spectrum of the vibrational modes is

$$\sum_{l'k'\beta}[M_{lk}\omega^2\delta_{ll'}\delta_{kk'}\delta_{\alpha\beta}-\phi_{\alpha\beta}(lk;l'k')]u_\beta(l'k')=0. \tag{2}$$

In the limiting cases at $c=0$ or $c=1$, Eq. (1) presents the Hamiltonian of the regular crystal with atoms B or A in the

corresponding sublattice. In this case all M_{lk}'s are l independent and equal to either M_B or M_A, and $\phi_{\alpha\beta}(lk;l'k') = \phi^0_{\alpha\beta}(lk;l'k')$ are the force constants for one of the pure crystals. Using the plane-wave representation for the atomic displacements,

$$u_\alpha(lk,t) = \frac{1}{N^{1/2}} \sum_{\mathbf{q},j} \left(\frac{\hbar}{2M_k \omega_j(\mathbf{q})} \right)^{1/2} w_\alpha(k|\mathbf{q}j) \times \exp[it\omega_j(\mathbf{q}) + i\mathbf{q}\mathbf{x}(lk)], \quad (3)$$

where summing is performed over the values of the wave vector $\mathbf{q}$ within the first Brillouin zone, and j is running over all modes of the vibrational spectrum of the lattice, we obtain the eigenfunctions $w_\alpha(k,\mathbf{q},j)$ of the equation of motion

$$\sum_{k'\beta} D_{\alpha\beta}(kk';\mathbf{q}) w_\beta(k'|\mathbf{q}j) = \omega_j(\mathbf{q})^2 w_\alpha(k,\mathbf{q},j), \quad (4)$$

where the matrix $D_{\alpha\beta}(kk';\mathbf{q})$ has rank $3r$ and is the Fourier transform of the dynamical matrix $D_{\alpha\beta}(lk;l'k')$ of the crystal

$$D_{\alpha\beta}(kk';\mathbf{q}) = \sum_{l,l'} D_{\alpha\beta}(lk;l'k') \exp\{i\mathbf{q}[\mathbf{x}(lk) - \mathbf{x}(l'k')]\}$$

$$= \frac{1}{(M_k M_{k'})^{1/2}} \sum_{l,l'} \phi^0_{\alpha\beta}(lk;l'k') \times \exp\{i\mathbf{q}[\mathbf{x}(lk) - \mathbf{x}(l'k')]\}. \quad (5)$$

Using the matrix notation, the equation of motion (2) for a pure crystal can be written as

$$\mathbf{L}\mathbf{u} = 0, \quad (6)$$

where the matrix $\mathbf{L}$ is defined by

$$L_{\alpha\beta}(lk,l'k') = M_k \omega^2 \delta_{ll'} \delta_{kk'} \delta_{\alpha\beta} - \phi^0_{\alpha\beta}(lk;l'k'). \quad (7)$$

We express the Green's function $\mathcal{G}^0_{\alpha\beta}(lk,l'k';\omega)$ of the pure crystal A or B which is a reciprocal matrix of $\mathbf{L}$ with the help of eigenfunctions $w_\alpha(k,\mathbf{q},j)$,

$$\mathcal{G}^0_{\alpha\beta}(lk,l'k';\omega) = \frac{1}{(M_k M_{k'})^{1/2}} G^0_{\alpha\beta}(lk,l'k';\omega), \quad (8)$$

where

$$G^0_{\alpha\beta}(lk,l'k';\omega) = \frac{1}{N} \sum_{\mathbf{q}j} \frac{w_\alpha(k|\mathbf{q},j) w^*_\beta(k'|\mathbf{q},j)}{\omega^2 - \omega_j^2(\mathbf{q}) - i0} \times e^{i\mathbf{q}[\mathbf{x}(lk) - \mathbf{x}(l'k')]}. \quad (9)$$

According to Ref. 4, the imaginary part of the diagonal matrix element of $G^0_{\alpha\beta}(lk,l'k';\omega)$ is related to the vibrational spectrum density of the crystal by

$$\rho^0(\omega) = \frac{2\omega}{\pi} \sum_{\alpha k} Im\, G^0_{\alpha\alpha}(lk,lk;\omega) = \frac{2\omega}{N} \sum_{\mathbf{q},j} \delta[\omega^2 - \omega_j^2(\mathbf{q})]$$

$$= \frac{\omega}{\pi N} \sum_{\mathbf{q},j} \int_{-\infty}^{\infty} e^{\{-iy[\omega^2 - \omega_j^2(\mathbf{q})]\}} dy, \quad (10)$$

where the normalization of $w_\alpha(k|\mathbf{q},j)$ is taken into account. The last expression can be rewritten as

$$\rho^0(\omega) = \frac{\omega}{\pi N} \sum_{\mathbf{q},j} \int_{-\infty}^{\infty} e^{\{-iy[\omega^2 \mathbf{I} - \mathbf{D}]_{\mathbf{q}j;\mathbf{q}j}\}} dy, \quad (11)$$

where

$$[\omega^2 \mathbf{I} - \mathbf{D}]_{\mathbf{q}j;\mathbf{q}j} = \sum_{\alpha k,\beta k'} w_\alpha(k|\mathbf{q},j)[\omega^2 \delta_{kk'} \delta_{\alpha\beta} - D_{\alpha\beta}(kk';\mathbf{q})] w^*_\beta(k'|\mathbf{q},j). \quad (12)$$

For a crystal with substitution defects the equation of motion[3–8] can be written as

$$[\mathbf{L} - \delta\mathbf{L}]\mathbf{u} = 0, \quad (13)$$

where matrix $\delta\mathbf{L}$ is

$$\delta L_{\alpha\beta}(lk;l'k') = (M_k - M_{lk})\omega^2 \delta_{ll'} \delta_{kk'} \delta_{\alpha\beta} - [\phi^0_{\alpha\beta}(lk;l'k') - \phi_{\alpha\beta}(lk;l'k')]. \quad (14)$$

The first term of the right-hand side of Eq. (14) presents perturbation by ''the mass defect,'' while the second term describes perturbation due to the difference in the force constants. Equation (13) can be transformed into

$$[\omega^2 \mathbf{I} - \mathbf{D} - \delta\mathbf{V}]\mathbf{v} = 0, \quad (15)$$

where

$$\delta V_{\alpha\beta}(lk;l'k') = M_k^{-1/2} \delta L_{\alpha\beta}(lk;l'k') M_{k'}^{-1/2}. \quad (16)$$

The DOS of a disordered crystal can be given by

$$\rho(\omega) = \frac{\omega}{\pi N} \sum_{\Lambda} \int_{-\infty}^{\infty} e^{\{-iy[\omega^2 \mathbf{I} - \mathbf{D} - \delta\mathbf{V}]_{\Lambda;\Lambda}\}} dy. \quad (17)$$

Here quantum numbers Λ enumerate the vibrational modes of the disordered crystal, and the matrix element

$$[\omega^2 \mathbf{I} - \mathbf{D} - \delta\mathbf{V}]_{\Lambda;\Lambda} = \sum_{\alpha lk,\beta l'k'} v_\alpha(lk|\Lambda)[\omega^2 \delta_{ll'} \delta_{kk'} \delta_{\alpha\beta} - D_{\alpha\beta}(lk;l'k') - \delta V_{\alpha\beta}(lk;l'k')] \times v^*_\beta(l'k'|\Lambda) \quad (18)$$

is an analog of the corresponding matrix element in Eq. (12). In this case it is defined with the help of eigenvectors of a defect crystal $v_\alpha(lk|\Lambda)$.

The equation

$$[\mathbf{I} - \mathbf{G}^0 \delta\mathbf{V}]\mathbf{v} = 0 \quad (19)$$

gives the frequencies and eigenvectors of the vibrations that are disturbed by the substitution. Here $\mathbf{G}^0$ is a reciprocal matrix of $[\omega^2\mathbf{I}-\mathbf{D}]$, and is defined by Eq. (9).

B. Localized states of disordered crystals

In considering the disorder effect due to mass perturbation, we can simplify our calculations of the vibrational spectrum by separating the perturbation $\delta\mathbf{L}$ into two parts

$$\delta\mathbf{L}=\langle\delta\mathbf{L}\rangle+[\delta\mathbf{L}-\langle\delta\mathbf{L}\rangle]=\langle\delta\mathbf{L}\rangle+\delta\mathbf{L}^{FL}. \tag{20}$$

Here $\langle\cdots\rangle$ denotes averaging over all possible configurations of the substitution atoms in their sublattice. The first term of Eq. (20) has the symmetry of an ideal lattice, and can be included into the matrix $\mathbf{L}$ of Eq. (7). This leads to the replacement of the atomic mass of the perturbed sublattice by its averaged l-independent value

$$\overline{M_k}=cM_A+(1-c)M_B. \tag{21}$$

As a result, we obtain the equation of motion in the averaged crystal approximation:

$$[\omega^2\mathbf{I}-\overline{\mathbf{D}}]\mathbf{e}=0. \tag{22}$$

The averaging procedure restores the lattice symmetry broken by the substitution and, as a consequence, the equation of motion can be solved by the methods used for an ideal crystal. This equation leads to the spectrum of the solid solution which is an interpolation between the spectra of the pure crystals containing atoms A and B.

The second term of Eq. (20) describes the fluctuation part of the perturbation. It is responsible for the scattering of the phonons obtained as a solution of Eq. (22) and, if the fluctuation-induced perturbation is strong enough, for a splitting off of the localized modes from the boundaries of the phonon bands. This aspect of the fluctuation effect is the subject of our consideration.

We consider the problem of a calculation of the density of localized states induced by fluctuations for the case when the number of fluctuations which are able to split off from a localized state remains small enough, and the resulting localized states can be treated in the zero approximation as isolated from each other. This situation can be reached in the limit of relatively low concentrations of the active component of a solid solution. The mathematically accurate criterion for this condition can be formulated for a random alloy by using the lattice percolation theory. Let us consider, as an example, a single-site perturbation. In the limit $c\to 0$ the alloy will mainly contain single defect atoms. Therefore, in this limit the problem is whether the perturbation is strong enough to split off the localized or gap state. This problem is closely related to the local perturbation problem solved in Ref. 38 for electrons, and in Refs. 3–6 for phonons (also see Refs. 7 and 8, and references therein).

If the averaged interatomic distances between substituted atoms A exceed the radius of the bound state appearing at each of the lattice sites occupied by atoms A, Eq. (19) reduces, with the accuracy up to the terms of the order of c^2, to the Koster-Slater-Lifshitz equation (see Refs. 3,5–8 and 38), which in our notation takes the form

$$[\mathbf{I}-\mathbf{G}^{av}(\omega)\,\delta\mathbf{V}^{FL}]\mathbf{v}=0, \tag{23}$$

where

$$\mathbf{G}^{av}(\omega)=[\omega^2\mathbf{I}-\overline{\mathbf{D}}]^{-1}, \tag{24}$$

The perturbation $\delta\mathbf{V}^{FL}$ is now embedded in the averaged crystal described by Eq. (22). For a single-site perturbation, the localized or gap state splits off the boundary of the vibration band if the perturbation in the lattice sites occupied by atoms A is large as compared with its critical magnitude, i.e.,

$$\delta\mathbf{V}^{FL}>[\mathbf{G}^{av}(\omega_B)]^{-1}, \tag{25}$$

where ω_B is the frequency of the vibrational band boundary. The critical value is defined here through the reciprocal value of the single site Green's function $G^{av}_{[\alpha\alpha llkk]}(\omega_B)$. Below we will find the critical condition for an arbitrary defect. If a localized state arises, the density of states is defined by the number of impurity atoms with an accuracy of the order of c^2. As c increases, clusters consisting of two and a larger number of atoms of the solid solution active component appear in the corresponding sublattice. The fluctuations will be represented by clusters consisting of a finite number of impurity atoms in the sublattice where the substitution takes place, until the critical concentration p_c is reached. Above the critical concentration, the so-called percolation cluster, which is extended over the whole crystal, evolves. The finite clusters above the critical concentration are placed within the holes of the percolation cluster, and their number decreases rapidly with a further increase in the concentration. The clusters of the site percolation problem are most important for the mass defect. The critical concentration for the fcc sublattice is about 20% and, therefore, at $c<0.2$ only clusters of finite size are responsible for the transformation of the vibrational spectrum of the solid solution.

The density of states of disordered systems can be found through the averaging procedure, i.e., by summing over the DOS corresponding to all possible realizations of the disorder with the weight multipliers P_Δ which are equal to the probability that a given variant of the random distribution occurs. Taking into account all of the possible quantum numbers Λ, we obtain

$$\rho(\omega)=\frac{\omega}{\pi N}\sum_\Lambda\int_{-\infty}^{\infty}\sum_\Delta P_\Delta\sum_\Lambda dy_\Lambda \times\exp\{-iy_\Lambda[\omega^2\mathbf{I}-\overline{\mathbf{D}}-\delta\mathbf{V}^{FL}]_{\Lambda\Lambda}\}. \tag{26}$$

Performing the integration over y_Λ, we transform $\rho(\omega)$ into

$$\rho(\omega)=2\omega\sum_\Delta P_\Delta\sum_\Lambda\delta(\omega^2-\omega^2_{\Delta\Lambda}). \tag{27}$$

Here we denote eigenvalues at a given realization of disorder by $\omega^2_{\Delta\Lambda}$.

C. Isolated cluster approximation at $c<p_c$, sum rule

Here we consider the problem in the limit $c<p_c$ when atoms A form only clusters of finite size. Let us assume that the cluster wave functions of the localized states do not overlap in the zero approximation, and treat the medium sur-

rounding the cluster in the averaged crystal approximation. The composition fluctuations outside the cluster will be considered later.

The equation of motion for a cluster can be presented in this approximation as

$$\{\mathbf{I}+\mathbf{g}^{av}(\omega)\,\delta\mathbf{V}^{FL}\}\mathbf{v}=0, \tag{28}$$

where $\mathbf{g}^{av}(\omega)$ is the fragment of the Green's-function matrix restricted by the region of the cluster $\mathcal{C}_{st,\kappa}$ consisting of s atoms A and t perimeter atoms B. Here index κ enumerates different spatial configurations of the cluster.

Using the approach developed in the theory of lattice dynamics,[5,6] we find the eigenfunctions and eigenvalues of the matrix

$$[\mathbf{g}^{av}(\omega)\,\delta\mathbf{V}^{FL}], \tag{29}$$

the rank of which is equal to the size of the cluster considered,

$$\sum_{\beta l' k' \in \mathcal{C}_{st,\kappa}} [\mathbf{g}^{av}(\omega)\,\delta\mathbf{V}]_{\alpha\beta lkl'k'}\Phi^{\sigma}_{\beta l' k'}(\omega)=\lambda^{\sigma}(\omega)\Phi^{\sigma}_{\alpha lk}(\omega), \tag{30}$$

where summing is performed over the region occupied by the cluster. The eigenfunctions form the complete orthonormal set of vectors obeying[5,6,39]

$$\sum_{\sigma}\Phi^{\sigma}_{\beta l' k'}\Phi^{\sigma}_{\alpha lk}(\omega)=\delta_{ll'}\delta_{kk'}\delta_{\alpha\beta}. \tag{31}$$

With the help of these eigenfunction and eigenvalues, the matrix $\{\mathbf{I}+\mathbf{g}^{av}(\omega)\,\delta\mathbf{V}\}^{-1}$ can be presented as

$$\{\mathbf{I}+\mathbf{g}^{av}(\omega)\boldsymbol{\Delta}\}^{-1}_{\alpha\beta lkl'k'}=\sum_{\sigma}\frac{\Phi^{\sigma}_{\alpha lk}(\omega)\Phi^{\sigma}_{\beta l' k'}(\omega)}{1-\lambda_{\sigma}(\omega)}. \tag{32}$$

The localized state will split off if at least for one of the σ's there exists a value $\omega=\omega_{loc}>0$ for which the equality

$$\lambda_{\sigma}(\omega_{loc})=1 \tag{33}$$

is fulfilled. As a rule, the nodeless state splits off first, and this state has the largest localization energy and is most important for the optical properties of a system. The eigenvectors of the localized states can be given by

$$\mathbf{v}^{\sigma}=\mathbf{G}^{av}(\omega)\boldsymbol{\Phi}^{\sigma}(\omega)\left|\boldsymbol{\Phi}^{\sigma}\mathbf{G}'^{av}(\omega)\boldsymbol{\Phi}^{\sigma}\right|^{-1/2}, \tag{34}$$

where

$$\mathbf{G}'^{av}(\omega)=\frac{\partial}{\partial\omega}\mathbf{G}^{av}(\omega).$$

The probability of realization of a cluster containing s atoms A and having a perimeter composed of t atoms B is

$$g_{st}c^{s}(1-c)^{t}, \tag{35}$$

where g_{st} is the number of different space configurations of the clusters with equal numbers of atoms A and B. Taking into account the nodeless bound states only, for the density of states we can write

$$\rho(\omega)=\frac{\omega}{\pi N}\sum_{s}\sum_{\kappa=1}^{g_{st}}c^{s}(1-c)^{t}\delta[\omega^2-(\omega^{st,\kappa}_{loc})^2]. \tag{36}$$

The integrated DOS per elementary cell can be written as

$$\mathcal{N}(0)=\int_0^{\Omega_L}\rho(\omega)d\omega=\sum_{st,\kappa}g_{st}c^{s}(1-c)^{t}=\sum_{s}n_s(c); \tag{37}$$

here Ω_L is the Lifshitz border for the given vibrational band which coincides with the band boundary of the pure crystal containing atoms A in the corresponding sublattice. The right-hand side of Eq. (37) coincides with the total number of clusters per sublattice site.

Sums similar to Eq. (37) are determined with sufficient accuracy by their lower limit, i.e., by their first few terms at any concentration. If a few first values of $n_s(c)$ are known for different lattices, Eq. (37) can be used to estimate the number of states split off from the band edge. The calculated nine $n_s(c)$'s for the fcc lattice are given in Ref. 24; the first four numbers are

$$n_1(c)=c(1-c)^{12},$$

$$n_2(c)=6c^2(1-c)^{18},$$

$$n_3(c)=c^3[8(1-c)^{22}+12(1-c)^{23}+30(1-c)^{24}],$$

$$n_4(c)=c^4[2(1-c)^{24}+27(1-c)^{26}+48(1-c)^{27}+96(1-c)^{28}+144(1-c)^{29}+158(1-c)^{30}].$$

Further useful information can be obtained if the dependence of the localization energy on the number of atoms A in a cluster is known, at least approximately. This allows us to estimate the energy dependence of the integrated DOS as well as of the DOS itself.

The maximum number of the localized states which can split off the cluster containing s attractive centers is equal to s. The mean numbers of clusters $n_s(c)$ of size s are normalized according to

$$N_A=N\sum_{s=1}^{\infty}n_s(c)s, \tag{38}$$

where N is the number of sublattice sites, and N_A is the mean number of atoms A per unit volume. This equation defines the upper limit of the number of localized states. This situation can be described as a case of separated bands at all finite concentrations of atoms A.

D. Effect of fluctuations on localized states of clusters

1. Fluctuations of the surrounding medium

In the previous consideration we supposed that the medium surrounding the clusters can be approximated by a virtual crystal. In order to estimate the role of the composition fluctuations outside the cluster we will substitute the obtained solution into Eq. (26), and find the first correction to the DOS due to fluctuations. As a result, we have

$$\rho(\omega)=\frac{\omega}{\pi N}\int_{-\infty}^{\infty}dy\sum_{s}\sum_{\kappa=1}^{g_{st}}c^{s}(1-c)^{t}\exp\{-iy[\omega^{2}-(\omega_{loc}^{st,\kappa})^{2}]\}\langle\exp\{-iy(\mathbf{v}^{st,\kappa}\delta\mathbf{V}^{FL}\mathbf{v}^{st,\kappa})\}\rangle, \quad (39)$$

where $\langle\cdots\rangle$ represents the averaging over all possible realizations of the lattice site filling except a given cluster. The matrix $\delta\mathbf{V}^{FL}$ for the mass defect for the lattice sites of the perturbed sublattice occupied by atoms A and B can be expressed as

$$\delta V_{\alpha\beta ll'kk'}^{FL}=\begin{cases}\left[\omega^{2}\dfrac{(1-c)\varepsilon}{(1+c\varepsilon)}\right]\delta_{\alpha\beta}\delta_{ll'}\delta_{kk'}\\ -\left[\omega^{2}\dfrac{c\varepsilon}{(1+c\varepsilon)}\right]\delta_{\alpha\beta}\delta_{ll'}\delta_{kk'},\end{cases} \quad (40)$$

where

$$\varepsilon=\frac{M_A-M_B}{M_B}.$$

For a random distribution, each of the perturbed sublattice sites is occupied by atom A or B with probability c or $(1-c)$, respectively. Taking into account that the averaged exponent is split into a product of exponents, and that each of the multipliers can be averaged independently, we obtain

$$\langle\exp\{-iy(\mathbf{v}^{st,\kappa}\delta\mathbf{V}^{FL}\mathbf{v}^{st,\kappa})\}\rangle=\prod_{lk\ni\mathcal{C}_{st,\kappa}}^{N}\left\{c\exp\left(-i\omega^{2}\frac{(1-c)\varepsilon}{(1+c\varepsilon)}|\mathbf{v}_{lk}^{st,\kappa}|^{2}y\right)+(1-c)\exp\left(i\omega^{2}\frac{c\varepsilon}{(1+c\varepsilon)}|\mathbf{v}_{lk}^{st,\kappa}|^{2}y\right)\right\}. \quad (41)$$

Here l and k take their values on the perturbed sublattice outside the cluster $\mathcal{C}_{st,\kappa}$. The averaged expression for the DOS can then be written as

$$\rho(\omega)=\frac{\omega}{\pi N}\int_{-\infty}^{\infty}dy\sum_{s}\sum_{\kappa=1}^{g_{st}}c^{s}(1-c)^{t}\times\exp\left\{-iy[\omega^{2}-(\omega_{loc}^{st,\kappa})^{2}]+\sum_{lk\ni\mathcal{C}_{st,\kappa}}\ln[R_{lk}(y)]\right\}, \quad (42)$$

where

$$R_{lk}(y)=\left\{c\exp\left(-i\omega^{2}\frac{(1-c)\varepsilon}{(1+c\varepsilon)}|\mathbf{v}_{lk}^{st,\kappa}|^{2}y\right)+(1-c)\exp\left(i\omega^{2}\frac{c\varepsilon}{(1+c\varepsilon)}|\mathbf{v}_{lk}^{st,\kappa}|^{2}y\right)\right\}. \quad (43)$$

Restricting to the first nonzero cumulant, for the DOS we have

$$\rho(\omega)=\frac{\omega}{\pi N}\int_{-\infty}^{\infty}dy\sum_{s}\sum_{\kappa=1}^{g_{st}}c^{s}(1-c)^{t}\times\exp\{-iy[\omega^{2}-(\omega_{loc}^{st,\kappa})^{2}]-\gamma_{st,\kappa}^{2}y^{2}/2\}, \quad (44)$$

where

$$\gamma_{st,\kappa}^{2}=\sum_{lk\ni\mathcal{C}_{st,\kappa}}\omega^{4}\frac{c(1-c)\varepsilon^{2}}{(1+c\varepsilon)^{2}}[|\mathbf{v}_{lk}^{st,\kappa}|^{2}]^{2}, \quad (45)$$

The summing in the last expression has to be performed over sublattice sites outside a given cluster. After calculating the integral over y, we have

$$\rho(\omega)=\sum_{s}\sum_{\kappa=1}^{g_{st}}c^{s}(1-c)^{t}\frac{1}{\sqrt{2\pi\gamma_{st,\kappa}^{2}}}\times\exp\{-[\omega^{2}-(\omega_{loc}^{st,\kappa})^{2}]^{2}/(2\gamma_{st,\kappa}^{2})\}. \quad (46)$$

The obtained expression differs from Eq. (36) because the localization energy in the last equation is defined with an accuracy $\gamma_{st,\kappa}$. If the localization energy and $\gamma_{st,\kappa}$ are comparable, the number of states split off from the band edge decreases due to fluctuations as compared to the case without fluctuations, and now

$$\mathcal{N}(0)=\int_{0}^{\Omega_{L}}\rho(\omega)d\omega\leqslant\sum_{s}n_{s}(c). \quad (47)$$

This means that fluctuations partially destroy the localized or gap states.

2. Fluctuations of the cluster's shape

Clusters of a large size s have a number of configurations[40] which increases exponentially with size. The variation of cluster shapes for a given s is accompanied by a change in their perimeter t. For equal s, the compact clusters have a minimal perimeter, while quasilinear clusters are characterized by the largest perimeters. The distribution of clusters over their perimeters for a given s have, with a high accuracy, a Gaussian form,[40] and can be given by

$$g_{st}\sim\exp\left[-\frac{(t-t_{max}^{s})^{2}}{2(\overline{\delta t})^{2}}\right]. \quad (48)$$

Here t_{max}^{s} is the value of the perimeter corresponding to the distribution maximum for a given s, and $(\overline{\delta t})$ is the distribution dispersion.

The complicated shapes of large clusters lead to the appearance of localized state whose wave functions do not spread over the whole cluster due to the quantum interference.[41] The localization energy is strongly dependent on the size of the cluster or its part if only a part of the cluster plays an active role in formation of the localized state. Therefore, the deepest localization energy for a given s must correspond to the compact clusters $\hbar\omega_{comp}^{s}$ where no interference effects are possible, while the clusters of a complicated shape will have a set of localization energies due to the quantum interference. The minimal size of the cluster fragment that can be separated by the interference is equal to a single atom, and the localization energy of such a fragment

in this conditions corresponds approximately to the localization energy of the cluster with $s=1$.[41] As a result, the cluster shape fluctuations should lead to a considerable dispersion of the localization energies at a fixed s:

$$\hbar\omega_{loc}^{s=1} \leqslant \hbar\omega_{loc}^{s} \leqslant \hbar\omega_{comp}^{s}. \tag{49}$$

The consequence that follows from Eqs. (48) and (49) is that the density of localized states $\rho_s(\omega_{loc}^s)$ of the cluster with a given s can be presented in a Gaussian form with a maximum near the localization energy $\hbar\omega_{loc}^s(t_{max}^s)$ corresponding to the most frequently occurring clusters,

$$\rho_s(\omega_{loc}^s) \sim \exp\left[-\frac{[\omega_{loc}^s-\omega_{loc}^s(t_{max}^s)]^2}{2(\overline{\delta\omega_{loc}^s})^2}\right], \tag{50}$$

which is broadened by a dispersion of the localization energy $\overline{\delta\omega_{loc}^s}$. Both the position of the maximum and the dispersion are restricted from above by the value of ω_{comp}^s

$$\omega_{loc}^{s=1} < \omega_{loc}^s(t_{max}^s) < \omega_{comp}^s, \quad \overline{\delta\omega_{loc}^s} < \omega_{comp}^s. \tag{51}$$

Our estimation of fluctuations of the cluster shapes and their effect on the density of localized or gap states for the large size clusters shows that localized states of large clusters must form a rather structureless background, while the band shape of the DOS is formed mainly by states of clusters of small and intermediate sizes.

For the clusters of small and intermediate size the role of fluctuations can be approximately estimated by extending the summing region in Eq. (45) over the region of the cluster itself,

$$\gamma_{st,\kappa}^2 = \sum_{lk} \omega^4 \frac{c(1-c)\varepsilon^2}{(1+c\varepsilon)^2}[|\mathbf{v}_{lk}^{st,\kappa}|^2]^2, \tag{52}$$

where composition fluctuations within the cluster are used instead of fluctuations of the cluster shape, because both kinds of fluctuations are characterized by the same variation in the perturbation energy. The obtained results provide the possibility to simulate the DOS of localized or gap states in a wide range of perturbation energies.

E. Continuum approach to the problem near the Van Hove critical points

This part of the paper is based on the results obtained for the electron spectrum of disordered systems in the region of localized states with the help of the so-called ''effective-mass'' approximation,[42–44] which can be introduced near the Van Hove critical points, first of all, above the maximum or below the minimum of the band in the band gap. There is an analogy in the behavior of electron and phonon band dispersions for ideal crystals, and the Taylor series expansion of the phonon branch curve has the same features in q space as the electron one (see Ref. 4, and references therein). The other characteristic of the approach is the use of the analogy between Mott's model[45] for a potential well or a barrier at the isoelectron substitution, and the perturbation of the vibrational motion by the mass defect.

1. Fourier representation of the equation of motion

We denote the eigenvalues of Eq. (22) as $\omega_j(c,\mathbf{q})$, where the dependence on the composition of the solid solution c is due to the averaged part of the perturbation $\langle\delta\mathbf{L}\rangle$. Using the eigenvectors of Eq. (22), $e_\alpha(k|\mathbf{q}j)$, as a basis for the representation of the wave function of the localized or gap state we take the solution of the equation in the form $\Sigma_j e_\alpha(k|\mathbf{q}j)\phi_\Lambda(lj)$, and obtain

$$[\omega^2\mathbf{I}-\overline{\mathbf{D}}-\delta\mathbf{V}^{FL}]\mathbf{e}\phi_\Lambda(lj)=0, \tag{53}$$

where $\phi_\Lambda(lj)$ is the enveloping wave function, and l runs over the perturbed sublattice sites. By multiplying the left-hand side of Eq. (53) by $\mathbf{e}$, we obtain

$$\{\omega^2-\omega_j^2(c,\mathbf{q})\}\phi_\Lambda(\mathbf{q}j)-\sum_{\mathbf{q}'j'}(\mathbf{e}\delta\mathbf{V}^{FL}\mathbf{e})_{\mathbf{q}\mathbf{q}'jj'}\phi_\Lambda(\mathbf{q}'j')=0. \tag{54}$$

Here $\phi_\Lambda(\mathbf{q}j)$ is the Fourier transform of the wave function, and

$$(\mathbf{e}\delta\mathbf{V}^{FL}\mathbf{e})_{\mathbf{q}\mathbf{q}'jj'}=\sum_{\alpha\beta ll'kk'} e_\alpha(k|\mathbf{q}j)\,\delta V_{\alpha\beta}^{FL} \times(lk;l'k')e_\beta^*(k'|\mathbf{q}'j')e^{i[\mathbf{q}\mathbf{x}(lk)-\mathbf{q}'\mathbf{x}(l'k')]}. \tag{55}$$

For a single-site mass defect,

$$(\mathbf{e}\delta\mathbf{V}^{FL}\mathbf{e})_{\mathbf{q}\mathbf{q}'jj'}=\sum_\alpha e_\alpha(k|\mathbf{q}j) \times\left[\omega^2\varepsilon\frac{(1-c)}{(1+c\varepsilon)}\right]e_\alpha^*(k|\mathbf{q}'j')e^{i[\mathbf{q}-\mathbf{q}']\mathbf{x}(lk)}. \tag{56}$$

The perturbation matrix contains both diagonal and off-diagonal elements with respect to indices j and j' even for a mass defect and, as a result, in the general case leads to the system of $3r$ equations of the type of Eq. (54).

2. Taylor series expansion near the Van Hove critical point

We consider Eq. (54) in the energy region just below the lowest Van Hove critical point of the j optical bands $\omega_j(c,\mathbf{q}_{cr})$ assuming that the localization energy is considerably lower than $\omega_j(c,\mathbf{q}_{cr})$. By performing the Taylor series expansion of $\omega_j^2(c,\mathbf{q}_{cr})$ up to the first nonzero term and preserving only the diagonal matrix element of the perturbation, we obtain the simplified expression

$$\left[\omega^2-\omega_j^2(c,\mathbf{q}_{cr})-\frac{1}{2}[\nabla_{\mathbf{q}}^2\omega_j^2(c,\mathbf{q}_{cr})](\mathbf{q}-\mathbf{q}_{cr})^2\right]\phi_\Lambda(\mathbf{q}j) -\sum_{\mathbf{q}'}(\mathbf{e}\delta\mathbf{V}^{FL}\mathbf{e})_{\mathbf{q}\mathbf{q}'jj}\phi_\Lambda(\mathbf{q}'j)=0. \tag{57}$$

Here

$$(\mathbf{e}\delta\mathbf{V}^{FL}\mathbf{e})_{\mathbf{q}\mathbf{q}'jj}=\sum_{\alpha\beta ll'kk'} e_\alpha(k|\mathbf{q}_{cr}j)\,\delta V^{FL}_{\alpha\beta} \times(lk;l'k')e^*_\beta(k'|\mathbf{q}_{cr}j)e^{i[\mathbf{q}\mathbf{x}(lk)-\mathbf{q}'\mathbf{x}(l'k')]}. \tag{58}$$

we used only the diagonal matrix element of the perturbation $(\mathbf{e}\delta\mathbf{V}^{FL}\mathbf{e})_{\mathbf{q}\mathbf{q}'jj}$, and the solution of Eq. (22), $e_\alpha(k|\mathbf{q}_{cr}j)$, at the critical point $\mathbf{q}_{cr}$. The amplitude of the perturbation for the cluster sites occupied by atoms A and B is defined now as

$$\delta V^{FL}_{\mathbf{q}\mathbf{q}'jj}=\begin{cases}\left[\omega_j^2(c,\mathbf{q}_{cr})\dfrac{(1-c)\varepsilon}{(1+c\varepsilon)}\right]|\mathbf{e}(k|\mathbf{q}_{cr}j|^2\\ -\left[\omega_j^2(c,\mathbf{q}_{cr})\dfrac{c\varepsilon}{(1+c\varepsilon)}\right]|\mathbf{e}(k|\mathbf{q}_{cr}j|^2\end{cases} \tag{59}$$

Taking into account the normalization of eigenvectors

$$\sum_k |\mathbf{e}(k|\mathbf{q}j|^2=1, \tag{60}$$

we see that the corresponding multiplier in Eq. (59) $|\mathbf{e}(k|\mathbf{q}_{cr}j|^2$, is less than unity, and for the wurtzite lattice with four atoms in the elementary cell it can be estimated as $\approx 1/4$. Therefore, this estimation, together with Eq. (59), gives the order of magnitude of the perturbation due to substitution.

The other estimation of the value of the perturbation for the mass defect near the critical point considered can be performed by using Eq. (22), which gives for $\mathbf{q}=\mathbf{q}_{cr}$ at $c=0$ and $c=1$ the values of $\omega_j(B,\mathbf{q}_{cr})$ and $\omega_j(A,\mathbf{q}_{cr})$ for the pure crystals BC and AC, respectively. Then, taking into account Eq. (21), for the composition shift of the critical point in the linear approximation we have

$$\Delta\omega_j^2(c\mathbf{q}_{cr})=[\omega_j^2(A,\mathbf{q}_{cr})-\omega_j^2(B,\mathbf{q}_{cr})]c, \tag{61}$$

while for the fluctuation part of perturbation we obtain, instead of Eq. (55), the following fluctuation ''potential'' amplitude

$$\langle\delta\mathbf{V}^{FL}\rangle_{kk|j,j}=\begin{cases}(1-c)[\omega_j^2(A,\mathbf{q}_{cr})-\omega_j^2(B,\mathbf{q}_{cr})]\\ -c[\omega_j^2(A,\mathbf{q}_{cr})-\omega_j^2(B,\mathbf{q}_{cr})].\end{cases} \tag{62}$$

This estimation gives for the perturbation approximately the same value as the previous one.

We define $v_0=V/N$ as the volume of a crystal per atom of a perturbed sublattice, assuming that there is a single atom of a given kind in the elementary cell. Then the first line of Eq. (62) gives the attractive part of the amplitude within the volume sv_0 for a given cluster, and the second line gives the repulsive amplitude of the barrier of volume, tv_0.

After the Fourier transformation of Eq. (57) into the continuum r space, we have

$$\left[\omega^2-\omega_j^2(c,\mathbf{q}_{cr})-\frac{1}{2}[\nabla^2_{\mathbf{q}}\omega_j^2(c,\mathbf{q}_{cr})]\nabla^2_{\mathbf{r}}\right]\phi_\Lambda(\mathbf{r}j) -(\mathbf{e}\delta\mathbf{V}^{FL}\mathbf{e})_{kk|j,j}(\mathbf{r})\,\phi_\Lambda(\mathbf{r}j)=0. \tag{63}$$

Here the last term of the equation is defined within the region occupied by a given cluster. Using the notation

$$-\omega^2+\omega_j^2(c,\mathbf{q}_{cr})=2\omega_j(c,\mathbf{q}_{cr})\omega_\Lambda, \quad M^j_{eff}=\frac{2\hbar\omega_j(c,\mathbf{q}_{cr})}{\nabla^2_{\mathbf{q}}\omega_j^2(c,\mathbf{q}_{cr})} \tag{64}$$

and

$$U^j_{eff}(r)=\frac{\hbar}{2\omega_j(c,\mathbf{q}_{cr})}(\mathbf{e}\delta\mathbf{V}^{FL}\mathbf{e})_{jj}(\mathbf{r}), \tag{65}$$

which for a mass defect has the form

$$U^j_{eff}(r)=\begin{cases}\dfrac{\hbar\omega_j(c,\mathbf{q}_{cr})(1-c)\varepsilon}{2(1+c\varepsilon)}|\mathbf{e}(k|\mathbf{q}_{cr}j)|^2\\ -\dfrac{\hbar\omega_j(c,\mathbf{q}_{cr})c\varepsilon}{2(1+c\varepsilon)}|\mathbf{e}(k|\mathbf{q}_{cr}j)|^2,\end{cases} \tag{66}$$

where the first line corresponds to the region occupied by the attractive atoms and the second line describes the repulsive barrier. We can write the equation of motion in the form of a Schrödinger equation:

$$\left\{-\frac{\hbar^2}{2M^j_{eff}}\nabla^2_{\mathbf{r}}+\omega_\Lambda-U^j_{eff}(r)\right\}\varphi_\Lambda(\mathbf{r}j)=0. \tag{67}$$

The cluster is described now by the potential well of volume sv_0 surrounded by the repulsive barrier having the volume tv_0. This fluctuation is embedded into the averaged medium.

In order to reconcile the lattice and continuum models, we define the critical value of the single site perturbation for the mass defect as

$$E_{cr}=\frac{\pi^2}{4}\frac{2\hbar\omega_j(c,\mathbf{q}_{cr})}{\nabla^2_{\mathbf{q}}\omega_j^2(c,\mathbf{q}_{cr})\left(\dfrac{3}{4\pi}v_0\right)^{2/3}}. \tag{68}$$

This is the critical value of the potential well depth for the well of volume v_0 in the averaged crystal, with a concentration c of atoms A. The lattice and continuum versions of the model will give approximately the same results if the relations between the perturbation amplitude and the critical value of the perturbation have the same order of magnitude. Note that both Eqs. (25) and (64) define the critical values of the perturbation without taking into account the repulsive barriers surrounding the clusters. The latter circumstance leads to an increase in the critical value of the perturbation.

The proposed model is, in its essence, the well-known Mott's model for an isoelectron substitution. Our consideration allows us to use it for the mass defect near the Van Hove singularity.

The value of the effective potential energy for a cluster within the potential attractive well formed by A atoms and within the repulsive barrier formed by atoms B can be defined with the help of Eq. (40) for a cluster of any size. A difficult problem is a great variety of cluster's spatial configurations. We simplify our calculations by using spherical potential wells whose volumes are equal to the volumes of corresponding clusters; to estimate barriers, we use the values of the parameter t averaged over cluster configurations.

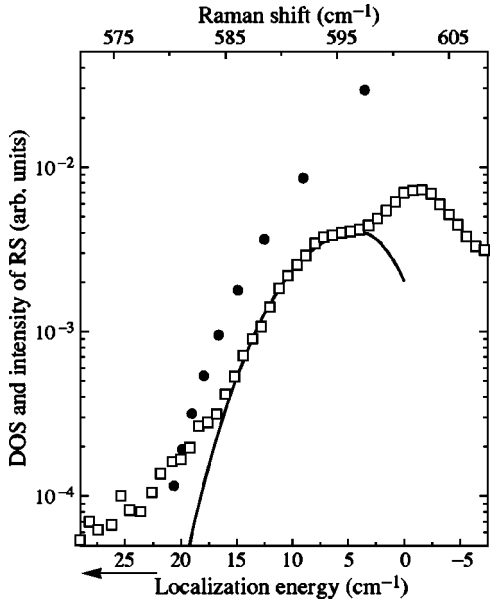

FIG. 7. The experimental Raman spectrum in the region of the gap mode for $c=0.08$ (squares), calculated DOS of the split-off states (solid line), and number of clusters per atom of cation sublattice for $s=1-9$ vs the localization energy of compact clusters (full circles).

3. Results of calculations

The results of calculations which take into account clusters with $s=1,\ldots,9$ are presented in Figs. 7, 8, and 9. Figures 7 and 8 show the densities of states for the gap states calculated through Eq. (46). It is seen that the experimental shape of the optical band coincides well with the calculated DOS. The effective potential amplitude used in calculation in both cases is equal to 32.5 cm^{-1}. This value is only about half the estimated magnitude in Eqs. (59) and (62). The ratio of the effective potential amplitude to the critical value of the potential was taken to be 1.55. The positions of the DOS maxima $\omega^s(\overline{t_{max}})$ for clusters with $s>3$ were taken to be $\omega^s_{comp}/2$. The most difficult problem is to find the acceptable estimates for broadening of the cluster bands. There are two additional reasons for the broadening not mentioned earlier. The first of these is that a real crystal has a lower symmetry and, therefore, the clusters regarded as identical in the cubic lattice become nonidentical in the wurtzite lattice with a corresponding change in the localization energy. This factor is of great importance for clusters with large s. The second reason is equally important for all of the clusters, and it is due to the anharmonic interaction of the lattice vibrations, which leads to a homogeneous broadening of the localized states. The large anharmonic broadening can completely or partially hide the inhomogeneous part of the band. The lack of reliable data on any structure of the gap bands makes it impossible to establish unambiguously all of the parameters of the problem. We have used these values to fit the band shape. To make the best-fit procedure more transparent, in Fig. 7 we give the spectrum of the gap states for broadening equal to the half of the broadenings in the final curve of this figure. Under this condition the broadening of the first maximum, which is due to clusters with $s=1$, coincides well with the estimate from Eq. (52), and we see the structure due to clusters $s=1-3$.

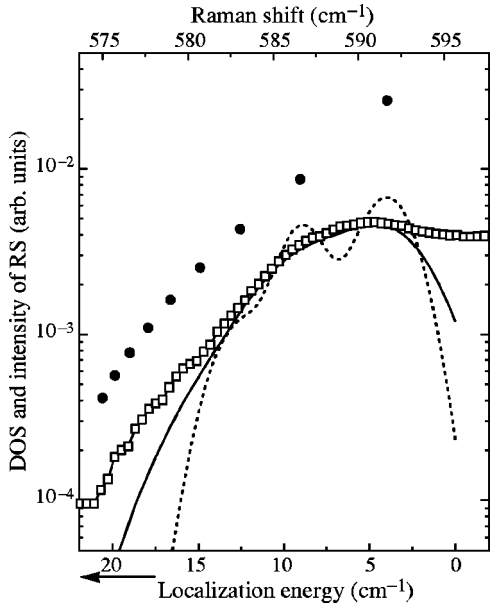

FIG. 8. The experimental Raman spectrum in the region of the gap mode for $c=0.13$ (squares), the calculated DOS of the split-off states (solid line), the DOS for broadenings equal to half of the best-fit values (dashed curve), and the number of clusters per atom of cation sublattice for $s=1-9$ vs the localization energy of compact clusters (full circles).

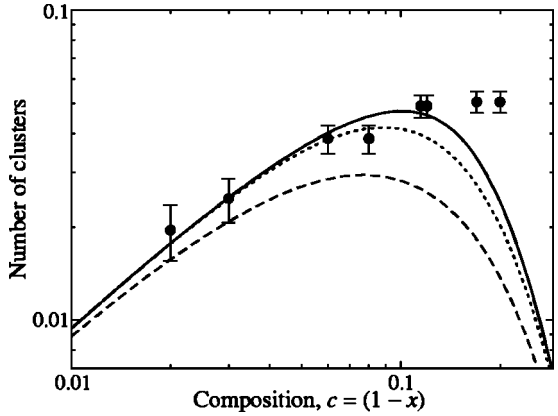

FIG. 9. The number of clusters per atom of cation sublattice for $s=1-3$ (dashed line), $s=1-5$ (dotted line), and $s=1-9$ (solid line) as a function of the composition of the solid solution, and the measured relative integral intensity of the A_1(TO) gap mode for different Ga concentrations (full circles).

Figure 9 gives the composition dependence of the integral intensity corresponding to the split-off states. We see that the satisfactory coincidence takes place in the region of concentrations below $c\leqslant 0.12-0.15$. A deviation of the experimental data from the calculated curves in the region $0.12-0.15\leqslant c<0.2$ can be partially due to a restriction on the size of clusters involved into calculations or due to the fact that ''percolation'' over the split-off cluster states can appear in the system. Under this condition the wave vector of the states above the percolation threshold, can be introduced, at least approximately. In this case the Raman intensity due to the states formed by clusters will be proportional to the spectral DOS with nearly zero wave vector. The behavior of the in-

tensity at $c>0.2$ demonstrates a relatively weak variation with composition which is consistent with the behavior of the spectral DOS.

A comparison of the composition dependence of DOS obtained for different numbers of clusters involved in calculations shows that the change in the curve is not considerable when the sum from Eq. (46) includes clusters with $s>5$. This result is a consequence of a rapid convergence of the sum in Eq. (37) known in the percolation theory. It is possible that inclusion of higher terms into calculations would lead to the occurrence of an almost horizontal region in the theoretical curve, which would improve the coincidence with experimental data, at least in the narrow interval just below the lattice percolation concentration.

V. SUMMARY REMARKS

Spectroscopic study of hexagonal $Al_xGa_{1-x}N$ alloys with a Ga content $(1-x)<0.3$ has revealed a large broadening of Raman spectrum in the region of an A_1(TO) optical branch accompanied by the appearance of a complex structure of the spectrum. The broadening of phonon bands of a disordered system occurs due to the violation of the wave-vector conservation law for both electronic and phonon systems. The manifestation of a phonon DOS in the region of the most low-frequency vibrations of the A_1(TO) optical branch can be regarded as a result of the considerable difference in masses of heavier Ga atoms substituting for Al. The detailed analysis performed in this paper has revealed that, simultaneously with the enhancement of this spectral region, the gap mode splits off at the band edge. This mode manifests itself as a relatively narrow peak at the low-energy edge of the A_1(TO) band. The relative intensity of the gap mode increases with increasing gallium content, and at Ga concentrations above $(1-x)=0.3$–0.4 it transforms into the A_1(TO) mode of the GaN crystal. Thus, in a limited range of Ga content, the behavior of the A_1(TO) phonon mode in $Al_xGa_{1-x}N$ can be considered a two-mode behavior.

The composition interval where the largest inhomogeneous broadening is observed, $(1-x)\approx 0.1$–0.25, includes the critical concentrations for the fcc sublattice both for percolation over sublattice sites $[(1-x)\approx 0.2]$ and percolation over bonds $[(1-x)\approx 0.12]$.

Changes in the vibration spectrum have been described using a theoretical model based on the microscopical approach. The experimental and theoretical dependences are in good agreement for the region $(1-x)\leqslant 0.12$–0.15. The obtained results indicate that the formation of the gap band A_1(TO) in the regions of low and intermediate concentrations can be explained by statistical clusters of Ga for the site percolation problem in the cation sublattice of the solid solution.

The suggested approach allows one to subdivide the entire compositional range of the solid solution into two parts. The first part is the region of very low Ga concentrations when only the isolated clusters of substituting atoms can exist. The wave functions of clusters in this region do not overlap, or can form only small complexes of clusters. The second region can be characterized by a sufficiently high concentration of clusters with overlapping wave functions, which leads to the formation of a ''percolation'' cluster extended over the whole crystal. Percolation over the split-off cluster states can arise in the system first in the region of the maximum density of these states. The critical concentration for the percolation can be considerably lower than the lattice critical concentration because of the large spatial extent of the cluster wave functions.

The obtained data seem to be insufficient to determine unambiguously the value of this percolation concentration and the position of the percolation threshold on the energy scale. The phonon states above the percolation threshold can move throughout the whole crystal, and can be characterized, at least approximately, by the wave vector. On the other hand, this means that the second mode in the vibrational spectrum of the solid solution occurs. To study this problem more thoroughly, experiments at He temperatures are needed to decrease the anharmonic broadening of the spectral peaks. Additional information can be obtained from luminescence spectra of deep centers.

The suggested approach can be useful for a more accurate description of the two-mode crystals and can serve as a background for using phenomenological methods in calculating vibrational spectra of disordered solid solutions. Note also that the two-mode-type behavior of the E_1(TO) and E_2(low) phonons have been revealed in this study as well. The behavior of these phonon modes and also of other modes in Al-rich hexagonal $Al_xGa_{1-x}N$ will be described in detail in a separate paper.

ACKNOWLEDGMENTS

This work was partly supported by RFBR (No. 99-02-18318) and the Program of the Ministry of Sciences of RF ''Physics of Solid State Nanostructures.''

[1] S. Nakamura, T. Mukai, and M. Senoh, Appl. Phys. Lett. **64**, 1687 (1994).
[2] S. Nakamura, M. Senoh, S. Nagahama, N. Iwasa, T. Yamada, T. Matsushita, H. Kiyoku, and Y. Sugimoto, Jpn. J. Appl. Phys. **35**, L74 (1996).
[3] I. M. Lifshitz, Nuovo Cimento Suppl. **3**, 716 (1956).
[4] A. A. Maradudin, E. W. Montroll, and G. N. Weiss, *Theory of Lattice Dynamics in the Harmonic Approximation* (Academic Press, New York, 1963).
[5] A. A. Maradudin, Rep. Prog. Phys. **XXVII**, 331 (1965).
[6] A. A. Maradudin, Solid State Phys. **18**, 273 (1966); **19**, 1 (1966).
[7] M. Lannoo and P. Lenglart, J. Phys. Chem. Solids **30**, 2409 (1969).
[8] J. Bernholc and Sokratas Pantelides, Phys. Rev. B **18**, 1780 (1978).
[9] R. J. Elliott, J. A. Krumhansl, and P. L. Leath, Rev. Mod. Phys. **46**, 465 (1974).
[10] I. F. Chang and S. S. Mitra, Phys. Rev. **172**, 924 (1968).
[11] I. F. Chang and S. S. Mitra, Adv. Phys. **20**, 359 (1971), and references therein.

[12] H. Grille and F. Bechstedt, J. Raman Spectrosc. **27**, 201 (1996).
[13] F. Bechstedt and H. Grille, Phys. Status Solidi B **216**, 761 (1999).
[14] H. Harima, T. Inoe, S. Nakashima, H. Okumura, Y. Ishida, S. Yoshida, T. Koizumi, H. Grille, and F. Bechstedt, Appl. Phys. Lett. **74**, 191 (1999).
[15] S. G. Yu, K. W. Kim, L. Bergman, M. Dutta, M. A. Stroscio, and J. M. Zavada, Phys. Rev. B **58**, 15 283 (1998).
[16] F. Demangeot, J. Groenen, J. Frandon, M. A. Renucci, O. Briot, S. Clur, and R. L. Aulombard, Appl. Phys. Lett. **72**, 2674 (1998).
[17] K. Hayashi, K. Itoh, N. Sawaki, and I. Akasaki, Solid State Commun. **77**, 115 (1991).
[18] D. Behr, R. Niebuhr, J. Wagner, K.-H. Bachem, and U. Kaufmann, Appl. Phys. Lett. **70**, 363 (1996).
[19] A. Cros, H. Angerer, R. Handschuh, O. Ambacher, and M. Stutzmann, Solid State Commun. **104**, 35 (1997).
[20] P. Wisniewski, W. Knap, J. P. Malzac, J. Camassel, M. D. Bremser, R. F. Davis, and T. Suski, Appl. Phys. Lett. **73**, 1760 (1998).
[21] J. W. Essam, in *Phase Transitions and Critical Phenomena*, edited by C. Domb and M. S. Green (Academic Press, London, 1972), Vol. 2, Chap. 6, p. 197.
[22] J. W. Essam, Rep. Prog. Phys. **43**, 833 (1980).
[23] A. Bunde and S. Havlin, in *Fractals and Disordered Systems*, edited by A. Bunde and S. Havlin (Springer-Verlag, Berlin, 1994), p. 51.
[24] M. F. Sykes, D. S. Gaunt, and M. Glen, J. Phys. A **9**, 1705 (1976).
[25] V. Yu. Davydov, I. N. Goncharuk, M. V. Baidakova, A. N. Smirnov, A. V. Subashiev, J. Aderhold, J. Stemmer, D. Uffmann, and O. Semchinova, Mater. Sci. Eng., B **59**, 222 (1999).
[26] Yu. V. Melnik, A. E. Nikolaev, S. I. Stepanov, A. S. Zubrilov, I. P. Nikitina, K. V. Vassilevski, D. V. Tsvetkov, A. I. Babanin, Yu. G. Musikhin, V. V. Tretyakov, and V. A. Dmitriev, in *Nitride Semiconductors*, edited by F. A. Ponve, S. D. Den Baars, B. K. Meyer, S. Nakamura, and S. Strite, MRS Symposia Proceedings No. 482 (Materials Research Society, Pittsburgh, 1998), p. 245.
[27] C. A. Arguello, D. L. Rousseau, and S. P. S. Porto, Phys. Rev. **181**, 1351 (1969).
[28] L. E. McNail, M. Grimsditch, and R. H. French, J. Am. Ceram. Soc. **76**, 1132 (1993).
[29] T. Azuhata, T. Sota, K. Suzuki, and S. Nakamura, J. Phys.: Condens. Matter **7**, L129 (1995).
[30] H. Siegle, G. Kaczmarczyk, L. Filippidis, A. P. Litvinchuk, A. Hoffmann, and C. Thomsen, Phys. Rev. B **55**, 7000 (1997).
[31] V. Yu. Davydov, Yu. E. Kitaev, I. N. Goncharuk, A. N. Smirnov, J. Graul, O. Semchinova, D. Uffmann, M. B. Smirnov, A. P. Mirgorodsky, and R. A. Evarestov, Phys. Rev. B **58**, 12 899 (1998).
[32] J. C. Nipko and C.-K. Loong, Phys. Rev. B **57**, 10 550 (1998); J. C. Nipko, C.-K. Loong, C. M. Balkas, and R. F. Davis, Appl. Phys. Lett. **73**, 34 (1998).
[33] K. Karch and F. Bechstedt, Phys. Rev. B **56**, 7404 (1997).
[34] S. Permogorov and A. Reznitsky, Solid State Commun. **18**, 781 (1976).
[35] M. Cardona, in *Light Scattering in Solids II*, edited by M. Cardona and G. Guntherodt, Topic in Applied Physics Vol. 50 (Springer, Berlin, 1982), p. 117.
[36] M. V. Belousov, in *Modern Problems in Condensed Matter Sciences, Vol. 2: Excitons*, edited by E. I. Rashba and M. D. Sturge (Publisher, City, 1982), p. 771.
[37] B. Velicky, S. Kirkpatrick, and H. Ehrenreich, Phys. Rev. **175**, 745 (1968).
[38] G. F. Koster and J. C. Slater, Phys. Rev. **95**, 1167 (1954).
[39] In general, we have to consider two sets of eigenvectors of matrix Eq. (29). Details can be found in Nguen Xuan Xinh, A. A. Maradudin, and R. A. Coldwell-Horsfall, J. Phys. (France) **26**, 717 (1965).
[40] A. Flammang, Z. Phys. B: Condens. Matter **28**, 47 (1977).
[41] S. Kirkpatrick and T. P. Eggarter, Phys. Rev. B **6**, 3598 (1972).
[42] A. A. Klochikhin and S. G. Ogloblin, Phys. Rev. B **48**, 3100 (1993).
[43] A. A. Klochikhin, Phys. Rev. B **52**, 10 979 (1995).
[44] A. Klochikhin, A. Reznitsky, S. Permogorov, T. Breitkopf, M. Grün, M. Hetterich, C. Klingshira, V. Lyssenko, W. Langbein, and J. M. Hvam, Phys. Rev. B **59**, 12 947 (1999).
[45] N. F. Mott, Proc. Cambridge Philos. Soc. **32**, 281 (1931).